Ternary Antimonides Yb*T*Sb (*T* = Ni, Pd, Pt, Cu, Ag, Au) – Synthesis, Structure, Homogeneity Ranges, and ^{121}Sb Mössbauer Spectroscopy

Ratikanta Mishra[a], Rainer Pöttgen[b], Rolf-Dieter Hoffmann[b], Thomas Fickenscher[b], Marcus Eschen[b], Henning Trill[c], and Bernd D. Mosel[c]

[a] Applied Chemistry Division, Bhabha Atomic Research Centre Trombay, Mumbai-400 085, India

[b] Institut für Anorganische und Analytische Chemie, Westfälische Wilhelms-Universität Münster, Wilhelm-Klemm-Strasse 8, D-48149 Münster, Germany

[c] Institut für Physikalische Chemie, Westfälische Wilhelms-Universität Münster, Schloßplatz 4/7, D-48149 Münster, Germany

Reprint requests to R. Pöttgen. E-mail: pottgen@uni-muenster.de

Z. Naturforsch. **57 b,** 1215–1223 (2002); received September 5, 2002

Antimony, Homogeneity Ranges, Mössbauer Spectroscopy

The ternary antimonides Yb*T*Sb (*T* = Ni, Pd, Pt, Cu, Ag, Au) were synthesized by reaction of the elements in sealed tantalum tubes in a high-frequency furnace. The structures of YbCuSb (NdPtSb type), YbAgSb (TiNiSi type), and YbAuSb (NdPtSb type) were confirmed on the basis of X-ray powder diffraction data. Those of the nickel, palladium, and platinum based antimonides (cubic MgAgAs type) were refined from single crystal X-ray data. The nickel based antimonide has a pronounced homogeneity range $YbNi_xSb$. The structures of five crystals have been investigated. The cubic lattice parameter increases with increasing nickel content from 613.13(6) pm (x = 0.17) to 621.25(5) pm (x = 0.63). Full occupancy of the palladium and antimony sites was observed for YbPdSb while the platinum compound shows some platinum vacancies leading to the composition $YbPt_{0.969(7)}Sb$ for the investigated crystal. A new, high-temperature modification of YbPdSb was obtained by rapidly quenching an arc-melted sample: TiNiSi type, *Pnma*, a = 725.6(2), b = 458.3(1), c = 785.4(2) pm, $wR2$ = 0.1255, 421 F^2 values, 20 variables. The antimonides Yb*T*Sb (*T* = Ni, Pd, Pt, Cu, Ag, Au) show single ^{121}Sb Mössbauer signals at isomer shifts ranging from –7.34 to –7.82 mm/s. The crystal chemistry and chemical bonding of these antimonides is discussed.

Introduction

The ternary equiatomic antimonides Yb*T*Sb (*T* = Ni, Pd, Pt, Cu, Ag, Au) have intensively been investigated in recent years with respect to their outstanding physical properties [1 - 24]. These antimonides crystallize with three different structure types. YbCuSb [6, 17, 19] and YbAuSb [6, 8, 17, 19] adopt the NdPtSb type [25], a slightly puckered variant of the AlB_2 structure [26] with an ordering of the transition metal and antimony atoms. In a recent X-ray powder diffraction study the ZrBeSi type was assigned to YbCuSb [19]. Here, the puckering of the [CuSb] network was not observed. The silver based antimonide crystallizes with the TiNiSi structure [27] which is an orthorhombically distorted superstructure of AlB_2 [26]. Based on the magnetic susceptibility and X-ray absorption spectroscopic measurements, a divalent ground state was found for the ytterbium atoms in these antimonides. In view of the absence of Sb-Sb bonding, the electron count may to a first approximation be written as $Yb^{2+}Cu^{+}Sb^{3-}$. YbCuSb, YbAgSb, and YbAuSb are metallic conductors [8, 17].

So far, the antimonides YbNiSb, YbPdSb, and YbPtSb [1 - 5, 7, 9 - 18, 19 - 24] were structurally characterized only on the basis of X-ray powder data. They adopt the cubic MgAgAs type structure [28], which may be considered as a filled version of YbSb [29] with NaCl structure. YbNiSb is a possible low-carrier heavy fermion compound. Magnetic ordering was detected below 0.85 K by ^{170}Yb Mössbauer spectroscopy. The spectra in the paramagnetic state show that the ytterbium site symmetry might deviate from O_h. Ytterbium / antimony disorder was discussed as a possible reason [15]. Furthermore, Skolozdra *et al.* reported on $YbNi_{0.9}Sb$ with a small nickel deficit which has a drastic ef-

Table 1. Lattice parameters, structure types, and space groups for the antimonides YbSb and Yb*T*Sb (*T* = Ni, Cu, Pd, Ag, Pt, Au).

Compd.	Type	SG	*a* (pm)	*b* (pm)	*c* (pm)	*V* (nm^3)	Ref.
YbSb	NaCl	*Fm3m*	608.2	*a*	*a*	0.2250	29
$YbNi_{0.17(2)}Sb$	BiF_3	*Fm3m*	613.13(6)	*a*	*a*	0.2305	this work
$YbNi_{0.25(13)}Sb$	BiF_3	*Fm3m*	613.67(7)	*a*	*a*	0.2311	this work
$YbNi_{0.39(3)}Sb$	BiF_3	*Fm3m*	617.85(6)	*a*	*a*	0.2359	this work
$YbNi_{0.55(4)}Sb$	BiF_3	*Fm3m*	619.51(6)	*a*	*a*	0.2378	this work
$YbNi_{0.63(2)}Sb$	BiF_3	*Fm3m*	621.25(5)	*a*	*a*	0.2398	this work
YbNiSb	MgAgAs	$F\bar{4}3m$	623.8	*a*	*a*	0.2427	20
YbNiSb	MgAgAs	$F\bar{4}3m$	624.23(1)	*a*	*a*	0.2432	15
YbCuSb	NdPtSb	$P6_3mc$	445.23(8)	*a*	796.7(1)	0.1368	this work
YbCuSb	Ni_2In	$P6_3/mmc$	445.6(1)	*a*	800.6(2)	0.1377	19
YbCuSb	NdPtSb	$P6_3mc$	445.2(1)	*a*	799.5(1)	0.1372	6
YbCuSb	NdPtSb	$P6_3mc$	444.8	*a*	791.6	0.1356	17
LT-YbPdSb	MgAgAs	$F\bar{4}3m$	645.58(5)	*a*	*a*	0.2691	this work
HT-YbPdSb	TiNiSi	*Pnma*	725.6(2)	458.3(1)	785.4(2)	0.2611	this work
YbPdSb	MgAgAs	$F\bar{4}3m$	647.1	*a*	*a*	0.2710	2
YbPdSb	MgAgAs	$F\bar{4}3m$	646.5(2)	*a*	*a*	0.2702	5
YbPdSb	MgAgAs	$F\bar{4}3m$	646.2	*a*	*a*	0.2698	3
YbPdSb	MgAgAs	$F\bar{4}3m$	645.3(1)	*a*	*a*	0.2687	16
YbAgSb	TiNiSi	*Pnma*	767.6(2)	462.5(1)	831.1(2)	0.2951	this work
YbAgSb	TiNiSi	*Pnma*	770.1	469.6	818.5	0.2960	17
YbAgSb	TiNiSi	*Pnma*	766.8(2)	459.6(1)	835.3(2)	0.2944	6
YbAgSb	TiNiSi	*Pnma*	766.8(3)	459.2(1)	837.8(4)	0.2950	19
YbPtSb	MgAgAs	$F\bar{4}3m$	646.24(6)	*a*	*a*	0.2699	this work
YbPtSb	MgAgAs	$F\bar{4}3m$	647.3	*a*	*a*	0.2712	17
YbAuSb	NdPtSb	$P6_3mc$	462.8(5)	*a*	775.4(5)	0.1438	this work
YbAuSb	NdPtSb	$P6_3mc$	461.9	*a*	776.8	0.1435	17
YbAuSb	NdPtSb	$P6_3mc$	463.9(1)	*a*	772.2(3)	0.1439	19
YbAuSb	NdPtSb	$P6_3mc$	463.5(1)	*a*	776.5(1)	0.1445	6

fect on the physical properties [20]. YbPdSb also has a $4f^{13}$ ground state. Magnetic ordering of the Yb^{3+} magnetic moments is evident below 1 K from ^{170}Yb Mössbauer spectroscopy. According to the high γ value (electronic specific heat coefficient) the palladium antimonide can also be classified as a heavy fermion material. Metallic YbPtSb shows Curie-Weiss behavior down to very low temperatures [7, 17]. So far, no magnetic ordering was detected. Since the ytterbium atoms are trivalent in Yb*T*Sb (*T* = Ni, Pd, Pt) and there exists no Sb-Sb bonding, the electron count may be written as $Yb^{3+}Ni^{\circ}Sb^{3-}$ etc.

In the present work we have investigated the structures of the cubic antimonides on the basis of single crystal X-ray data. Especially for the nickel compound we could show that a significant homogeneity range $YbNi_{1-x}Sb$ exists, strongly supporting the observations of Skolozdra *et al.* [20]. Furthermore, we investigated all Yb*T*Sb antimonides by ^{121}Sb Mössbauer spectroscopy, and we found a new orthorhombic high-temperature modification of YbPdSb.

Experimental Section

Synthesis

Starting materials for the preparation of the antimonides Yb*T*Sb (*T* = Ni, Pd, Pt, Cu, Ag, Au) were sublimed ingots of ytterbium (Johnson Matthey), silver and gold wire (Degussa-Hüls, ø 1 mm), nickel wire (Johnson Matthey, ø 0.38 mm), copper wire (Johnson Matthey, ø 1 mm), palladium and platinum powder (Degussa-Hüls, 200 mesh), and antimony lumps (Johnson Matthey), all with stated purities better than 99.9%. The samples of Yb*T*Sb (*T* = Ni, Pd, Pt, Cu, Ag, Au) were prepared in sealed tantalum tubes. Pieces of ytterbium, the transition metal powder or wire and the antimony lumps were mixed in the ideal 1:1:1 atomic ratio and sealed in small tantalum tubes (tube volume about 1 cm^3) under an argon atmosphere of about 800 mbar [30]. The argon was purified

Table 2. Crystal data and structure refinement for $YbNi_{0.17(2)}Sb$, $YbNi_{0.25(13)}Sb$, $YbNi_{0.39(3)}Sb$, and $YbNi_{0.55(4)}Sb$ (space group $Fm3m$, $Z = 4$).

Empirical formula	$YbNi_{0.17(2)}Sb$	$YbNi_{0.25(13)}Sb$	$YbNi_{0.39(3)}Sb$	$YbNi_{0.55(4)}Sb$
Molar mass	304.92 g/mol	309.47 g/mol	317.69 g/mol	327.08 g/mol
Unit cell dimensions	a = 613.13(6) pm	a = 613.67(7) pm	a = 617.85(6) pm	a = 619.51(6) pm
	V = 0.2305 nm^3	V = 0.2311 nm^3	V = 0.2359 nm^3	V = 0.2378 nm^3
Calculated density	8.79 g/cm^3	8.89 g/cm^3	8.95 g/cm^3	9.14 g/cm^3
Crystal size	30 × 30 × 60 μm^3	20 × 30 × 40 μm^3	20 × 20 × 60 μm^3	60 × 60 × 60 μm^3
Transm. ratio (max/min)	2.47	1.91	1.65	1.90
Absorption coefficient	52.9 mm^{-1}	53.4 mm^{-1}	53.4 mm^{-1}	54.2 mm^{-1}
F(000)	503	512	528	546
θ Range	5° to 45°	5° to 30°	5° to 40°	5° to 35°
Range in hkl	±12, ±12, +12	±8, ±8, ±8	±11, ±11, +9	±9, ±9, ±9
Total no. reflections	1018	594	748	1036
Independent reflections	74 (R_{int} = 0.1410)	33 (R_{int} = 0.2509)	58 (R_{int} = 0.0733)	44 (R_{int} = 0.0467)
Reflections with $I > 2\sigma(I)$	52 (R_{sigma} = 0.0391)	28 (R_{sigma} = 0.0893)	45 (R_{sigma} = 0.0225)	43 (R_{sigma} = 0.0121)
Data / parameters	74 / 6	33 / 6	58 / 6	44 / 6
Goodness-of-fit on F^2	1.000	1.182	1.107	1.269
Final R indices [$I > 2\sigma(I)$]	$R1$ = 0.0214	$R1$ = 0.0303	$R1$ = 0.0188	$R1$ = 0.0149
	$wR2$ = 0.0318	$wR2$ = 0.0680	$wR2$ = 0.0398	$wR2$ = 0.0415
R Indices (all data)	$R1$ = 0.0465	$R1$ = 0.0367	$R1$ = 0.0288	$R1$ = 0.0157
	$wR2$ = 0.0353	$wR2$ = 0.0732	$wR2$ = 0.0422	$wR2$ = 0.0425
Extinction coefficient	0.0008(2)	0.001(1)	0.0034(5)	0.018(2)
Largest diff. peak and hole	2.85 and –1.57 e/Å^3	2.40 and –1.64 e/Å^3	1.21 and –1.64 e/Å^3	1.22 and –1.03 e/Å^3

Table 3. Crystal data and structure refinement for $YbNi_{0.63(2)}Sb$, LT-YbPdSb, HT-YbPdSb, and $YbPt_{0.969(7)}Sb$.

Empirical formula	$YbNi_{0.63(2)}Sb$	LT-YbPdSb	HT-YbPdSb	$YbPt_{0.969(7)}Sb$
Molar mass	331.78 g/mol	401.19 g/mol	401.19 g/mol	489.88 g/mol
Unit cell dimensions	a = 621.25(5) pm	a = 645.58(5) pm	a = 725.6(2) pm	a = 646.24(6) pm
	$b = a$	$b = a$	b = 458.3(1) pm	$b = a$
	$c = a$	$c = a$	c = 785.4(2) pm	$c = a$
	V = 0.2398 nm^3	V = 0.2691 nm^3	V = 0.2612 nm^3	V = 0.2699 nm^3
Space group	$Fm3m$ (No. 225)	$F\bar{4}3m$ (No. 216)	$Pnma$ (No. 62)	$F\bar{4}3m$ (No. 216)
Formula unit per cell	$Z = 4$	$Z = 4$	$Z = 4$	$Z = 4$
Calculated density	9.19 g/cm^3	9.90 g/cm^3	10.20 g/cm^3	12.06 g/cm^3
Crystal size	15 × 20 × 30 μm^3	45 × 60 × 80 μm^3	5 × 40 × 55 μm^3	20 × 35 × 40 μm^3
Transm. ratio (max/min)	1.19	2.32	2.02	1.65
Absorption coefficient	54.4 mm^{-1}	50.7 mm^{-1}	52.2 mm^{-1}	95.6 mm^{-1}
F(000)	555	668	668	796
θ Range	5° to 40°	5° to 35°	3° to 30°	5° to 45°
Range in hkl	±11, ±11, +7	±10, ±10, ±10	±10, +6, ±11	±12, ±12, +12
Total no. reflections	650	791	1567	1268
Independent reflections	58 (R_{int} = 0.1178)	70 (R_{int} = 0.0583)	421 (R_{int} = 0.1112)	144 (R_{int} = 0.1163)
Reflections with $I > 2\sigma(I)$	43 (R_{sigma} = 0.0411)	70 (R_{sigma} = 0.0223)	266 (R_{sigma} = 0.0750)	138 (R_{sigma} = 0.0473)
Data/parameters	58 / 6	70 / 5	421 / 20	144 / 7
Goodness-of-fit on F^2	1.118	1.248	1.100	1.137
Final R indices [$I > 2\sigma(I)$]	$R1$ = 0.0235	$R1$ = 0.0205	$R1$ = 0.0565	$R1$ = 0.0305
	$wR2$ = 0.0271	$wR2$ = 0.0476	$wR2$ = 0.1060	$wR2$ = 0.0632
R Indices (all data)	$R1$ = 0.0573	$R1$ = 0.0205	$R1$ = 0.1068	$R1$ = 0.0333
	$wR2$ = 0.0323	$wR2$ = 0.0476	$wR2$ = 0.1255	$wR2$ = 0.0648
Flack parameter	–	–0.03(2)	–	–0.01(6)
Extinction coefficient	0.0018(3)	0.003(2)	0.0021(5)	0.0074(7)
Largest diff. peak and hole	2.08 and –3.20 e/Å^3	1.81 and –2.30 e/Å^3	4.93 and –3.41 e/Å^3	2.58 and –2.51 e/Å^3

over titanium sponge (900 K), silica gel, and molecular sieves.

The tantalum tubes were placed in a water-cooled quartz glass sample chamber in a high-frequency furnace (KONTRON Roto-Melt, 1.2 kW) under flowing argon [31]. They were first heated for 1 min with the maximum power output (about 1500 K), cooled to about 1100 K and heated again to the maximum. Subsequently the tubes were annealed at about 900 K for another 4 h. After the annealing procedures the samples could easily be separated from the tantalum tubes. No reactions of the samples with the tubes could be detected. Compact pieces are light gray with metallic luster. The samples are stable in moist air.

Some samples of YbPdSb quenched from high temperatures showed additional reflections which could be indexed on the basis of a primitive orthorhombic cell. This was indicative for a phase transition. We have subsequently cold-pressed parts of the cubic YbPdSb samples into small pellets (ø 6 mm, 1 mm height) which were arc-melted under an argon atmosphere of 600 mbar. Due to the small sample size it was possible to rapidly quench the high temperature phase. Nevertheless, we could not quench the samples rapidly enough to obtain single phase materials of the high temperature phase.

X-ray investigations

All samples were characterized through powder diffractograms (Stoe StadiP) or Guinier patterns using Cu-K_{α_1} radiation and silicon (a = 543.07 pm) or α-quartz (a = 491.30, c = 540.46 pm) as external or internal standard, respectively. The lattice parameters (Table 1) were obtained from least-squares fits of the powder data. The correct indexing of the patterns was facilitated by intensity calculations [32] taking the atomic positions from the structure refinements. For comparison, the lattice parameters given in the previous literature are also listed in that Table. Due to the large homogeneity range, for the $YbNi_xSb$ crystals we used the single crystal lattice parameters.

Silvery, irregularly shaped single crystals of YbPdSb, YbPtSb and the various $YbNi_xSb$ samples were isolated from the annealed samples by mechanical fragmentation. They were examined on a Buerger precession camera equipped with an image plate system (Fujifilm BAS-2500) in order to establish suitability for intensity data collection.

Single crystal intensity data of most compounds were collected at room temperature by use of a four-circle diffractometer (CAD4) with graphite monochromatized Mo-K_α radiation (71.073 pm) and a scintillation counter with pulse height discrimination. The scans were performed in the $\omega/2\theta$ mode. Empirical absorption corrections were applied on the basis of Ψ-scan data. The data set of cubic YbPdSb was collected on a Stoe IPDS-II image plate diffractometer at a detector distance of 60 mm, an exposure time of 10 min, and an omega range from 0 to 180° ($\Delta\omega$ = 1°). The integration parameters were A = 14.9, B = 6.7, and EMS = 0.029. The crystal of $YbNi_{0.25}Sb$ was measured on a Stoe IPDS-I diffractometer (50 mm detector distance, phi range 0 - 180°; $\Delta\varphi$ 1.4°, 6 min, profile/pixel 9/25; ems 0.016). A numerical absorption correction was applied to the data. All relevant crystallographic data and experimental details for the data collections are listed in Tables 2 and 3.

Table 4. Occupancy of the transition metal (*T*) positions and isotropic displacement parameters for the cubic antimonides Yb*T*Sb. The structures of the nickel compounds have been refined in space group *Fm*3*m* (Yb: 4*a*, Ni: 8*c*, Sb: 4*b*) with a statistical nickel occupancy, while YbPdSb and $YbPt_{0.969(7)}Sb$ show ordered structures (space group $F\bar{4}3m$, Yb: 4a, *T*: 4*c*, Sb: 4*b*). For details see text.

Compound	*T* Occupancy/%	U_{eq}(Yb)	U_{eq}(*T*)	U_{eq}(Sb)
$YbNi_{0.17(2)}Sb$	17(2)	137(4)	86(36)	103(4)
$YbNi_{0.25(13)}Sb$	25(13)	134(11)	260(247)	85(8)
$YbNi_{0.39(3)}Sb$	39(3)	176(4)	135(25)	149(4)
$YbNi_{0.55(4)}Sb$	55(4)	202(5)	173(29)	183(5)
$YbNi_{0.63(2)}Sb$	63(2)	147(5)	95(15)	153(6)
YbPdSb	100	75(4)	95(4)	61(4)
$YbPt_{0.969(7)}Sb$	96.9(7)	65(5)	65(3)	55(6)

Structure refinements

Analyses of the systematic extinctions led to space groups $F\bar{4}3m$ for Yb*T*Sb (T = Pd, Pt) and *Pnma* for the high temperature modification (HT) of YbPdSb. The nickel based antimonides showed all statistical occupancy. Therefore these structures have been refined in space group *Fm*3*m*. All atoms of the cubic structures lie on special positions. The starting atomic parameters for HT-YbPdSb were deduced from an automatic interpretation of direct methods with SHELXS-97 [33]. The structures were refined using SHELXL-97 (full-matrix least-squares on F_o^2) [34] with anisotropic atomic displacement parameters for all atoms. The nickel occupancy parameters of $YbNi_xSb$ and the platinum occupancy parameter of $YbPt_{0.969(7)}Sb$ have been refined as a least squares variable. All other sites are fully occupied within two standard deviations. No Pd-Sb mixing is evident from the X-ray data of HT-YbPdSb. The refined occupancy parameters are 99.6(19)% for Pd and 99.7(16)% for Sb. Ideal occupancies have been assumed in the final cycles. Final difference Fourier syntheses revealed no significant resid-

Table 5. Atomic coordinates and anisotropic displacement parameters (pm^2) for the orthorhombic high temperature modification of YbPdSb, space group *Pnma*. U_{eq} is defined as one third of the trace of the orthogonalized U_{ij} tensor. $U_{23} = U_{12} = 0$.

Atom	Wyckoff position	*x*	*y*	*z*	U_{11}	U_{22}	U_{33}	U_{13}	U_{eq}
Yb	4*c*	0.9969(3)	1/4	0.7067(2)	100(6)	144(7)	137(7)	–17(7)	127(4)
Pd	4*c*	0.1859(4)	1/4	0.0785(4)	185(15)	118(16)	142(15)	–1(11)	148(7)
Sb	4*c*	0.2922(3)	1/4	0.4059(3)	160(12)	123(14)	84(11)	1(9)	122(6)

Table 6. Interatomic distances (pm), calculated with the lattice parameters taken from X-ray powder data of LT-YbPdSn and HT-YbPdSb. All distances within the first coordination spheres are listed. Standard deviations are equal or less than 0.4 pm.

LT-YbPdSb (MgAgAs type):

Yb:	4	Pd	279.5	Pd:	4	Sb	279.5	Sb:	4	Pd	279.5
	6	Sb	322.8		4	Yb	279.5		6	Yb	322.8
	12	Yb	456.5								

HT-YbPdSb (TiNiSi type):

Yb:	2	Pd	314.0	Pd:	2	Sb	266.7	Sb:	2	Pd	266.7
	2	Sb	316.9		1	Sb	268.5		1	Pd	268.5
	1	Pd	318.0		1	Sb	285.9		1	Pd	285.9
	1	Sb	319.0		2	Yb	314.0		2	Yb	316.9
	1	Pd	322.6		1	Yb	318.0		1	Yb	319.0
	2	Sb	323.1		1	Yb	322.6		2	Yb	323.1
	1	Sb	338.5		2	Yb	340.0		1	Yb	338.5
	2	Pd	340.0								
	2	Yb	369.1								
	2	Yb	397.4								

ual peaks (see Tables 2 and 3). The positional parameters and interatomic distances of the refinements are listed in Tables 4 - 6. Listings of the observed and calculated structure factors are available*.

^{121}Sb Mössbauer spectroscopy

A $Ba^{121m}SnO_3$ source was used for the Mössbauer spectroscopic experiments. The measurements were carried out in a helium bath cryostat at 78 K. The temperature was controlled by a resistance thermometer (±0.5 K accuracy). The Mössbauer source was kept at room temperature. The samples were enclosed in small PVC containers at a thickness corresponding to about 10 mg Sb/cm^2.

*Details may be obtained from: Fachinformationszentrum Karlsruhe, D-76344 Eggenstein-Leopoldshafen (Germany), by quoting the Registry No's. CSD-391177 ($YbNi_{0.17}Sb$), CSD-391187 ($YbNi_{0.25}Sb$), CSD-391186 ($YbNi_{0.39}Sb$), CSD-391185 ($YbNi_{0.55}Sb$), CSD-391184 ($YbNi_{0.63}Sb$), CSD-391183 (cubic-YbPdSb), CSD-391182 (orthorhombic YbPdSb), and CSD-391181 (YbPtSb).

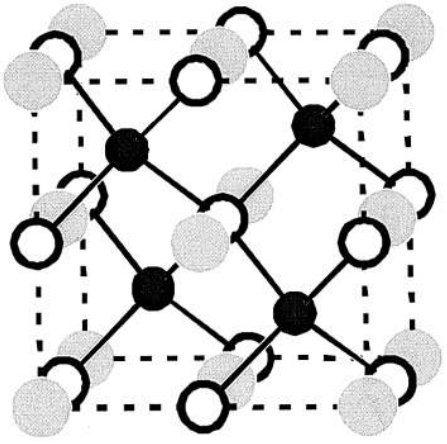

Fig. 1. The crystal structure of LT-YbPdSb. Ytterbium, palladium, and antimony atoms are drawn as gray, filled, and open circles, respectively. The three-dimensional [PdSb] network is emphasized.

Discussion

Crystal chemistry

The equiatomic antimonides Yb*T*Sb (*T* = Ni, Pd, Pt, Cu, Ag, Au) have been known for a long time. First reports on YbNiSb and YbPtSb were given by Dwight [1] almost thirty years ago. In recent years the structures of the copper, silver, and gold compound have been investigated on the basis of X-ray single crystal data and Rietveld refinements [6, 17, 19]. Our X-ray powder data are in good agreement with these findings. In contrast, no precise structural data are known for Yb*T*Sb (*T* = Ni, Pd, Pt). All reports are based on X-ray powder data.

^{170}Yb Mössbauer spectra of YbNiSb and YbPdSb [10, 14 - 16] showed a significantly different behavior. Above 1.4 K YbPdSb shows one-line spectra [10, 14, 16] while the YbNiSb samples show a sizeable distribution of crystal field distortions which lead to a distribution of crystal electric field energies [15]. The authors discussed these results in the context of possible atomic disorder and / or struc-

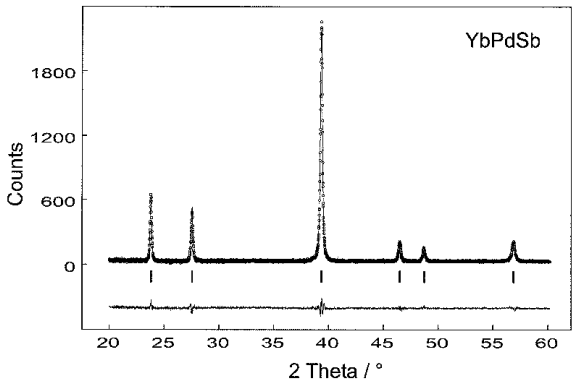

Fig. 2. Experimental and simulated X-ray powder pattern of LT-YbPdSb (Cu-K_{α_1} radiation).

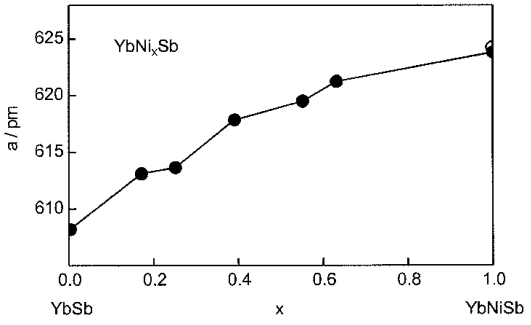

Fig. 3. Variation of the cubic lattice parameter within the solid solution YbNi$_x$Sb.

tural phase transitions. In view of these results it was desirable to refine the Yb*T*Sb (*T* = Ni, Pd, Pt) structures from X-ray single crystal data in order to get more reliable structural information.

Refinement of the cubic YbPdSb structure (MgAgAs type, space group $F\bar{4}3m$, Fig. 1) showed no anomalies. The X-ray powder pattern (Fig. 2) showed perfect line shapes and the refined occupancy parameters indicated the ideal composition. The structure can be described in two ways. Ytterbium and antimony atoms build a NaCl type substructure in which the palladium atoms fill one half of the tetrahedral voids in an ordered manner. A binary antimonide YbSb with rocksalt structure is known indeed [29]. Alternatively, the palladium and antimony atoms build a blende type [PdSb] substructure in which the ytterbium atoms are located. The binary representatives for this structure type are BiF_3 [35] and Li_3Bi [36].

The results were different for the nickel containing systems. In contrast to the palladium based crystals we found a partial occupancy of the nickel sites. Due to this statistic, these structures have been refined in the higher symmetric space group *Fm*3*m*. The nickel atoms partially fill the tetrahedral voids of the YbSb substructure. As outlined in Fig. 3, the *a* lattice parameter increases with increasing nickel content. The structures of five YbNi$_x$Sb crystals with different nickel contents have been refined. In contrast to the ideal line shape for the YbPdSb pattern, we observe a significant tailing of the reflections for the various YbNiSb samples. Exemplarily we present the shape of the *220* reflection in Fig. 4. We interpret this result in the following way: The YbNiSb samples contain about 90% of the more or less stoichiometric 1:1:1 compound and about 10% of a distribution of different YbNi$_x$Sb stochiometry ($x < 1$). The main part of the reflections always occurs at the same 2θ positions. The tailing of the reflections corresponds to parts of the samples with smaller lattice parameters, *i. e.* lower nickel contents. The varying nickel content has a large influence on the electronic state of the ytterbium atoms and thus on the Mössbauer behavior. The ^{170}Yb Mössbauer spectra presented in [15] are certainly a superposition of a main line corresponding to stoichiometric YbNiSb and a distribution of signals originating from YbNi$_x$Sb. At this point we should clearly state that there seems to be no deviation from cubic symmetry.

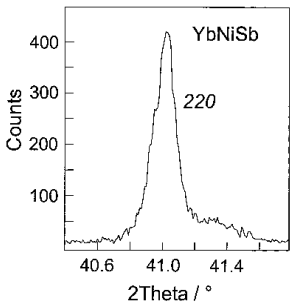

Fig. 4. Profile of a 220 reflection of a typical YbNiSb sample.

The situation seems to be even more complex for YbPdBi. A very large variation of the cubic lattice parameters has been reported [24]: 654.7 - 661.25 pm. This behavior is either indicative for Pd-Bi mixing or a homogeneity range YbPd$_x$Bi, similar to YbNi$_x$Sb.

Detailed electronic structure calculations on stoichiometric YbNiSb have recently been carried out

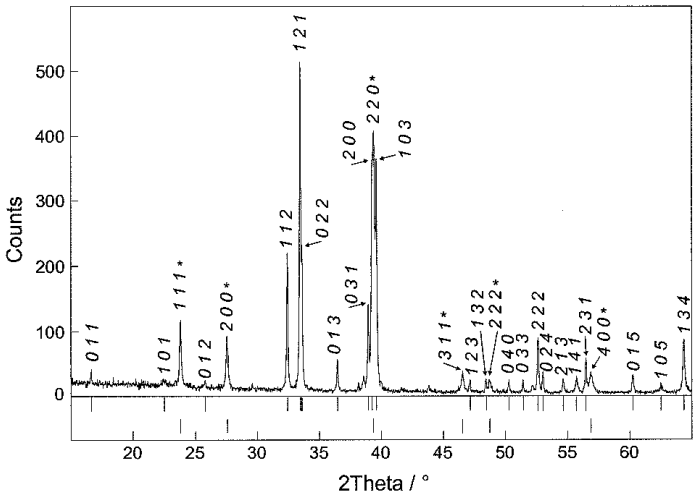

Fig. 5. X-ray powder pattern (Cu-K_{α_1} radiation) of a mixture of LT- and HT-YbPdSb. The *hkl* indices and line positions of both phases are given with the cubic ones marked by asterisks. Small impurity lines occur around 38° and 44°.

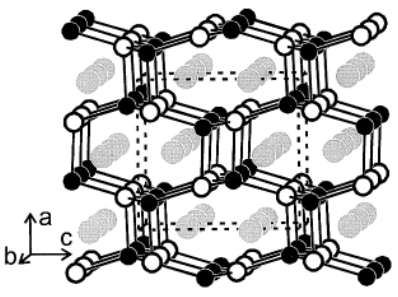

Fig. 6. Crystal structure of HT-YbPdSb (TiNiSi type). Ytterbium, palladium, and antimony atoms are drawn as gray, filled, and open circles, respectively. The three-dimensional [PdSb] network is emphasized.

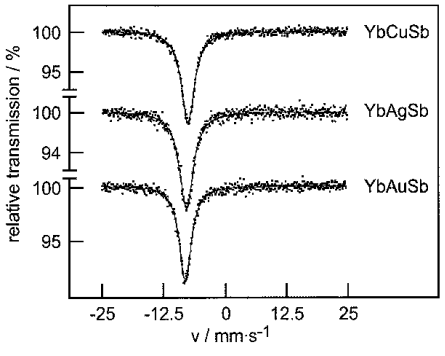

Fig. 7. Experimental and simulated ^{121}Sb Mössbauer spectra of Yb*T*Sb (*T* = Cu, Ag, Au) at 78 K.

by Kanatzidis and coworkers [21, 22]. We refer to this work for further information.

Quenching of the palladium based samples from high temperature (HT) resulted in a two-phase sample. Besides cubic LT-YbPdSb we observed HT-YbPdSb with the orthorhombic TiNiSi type structure. This was already evident from the X-ray powder pattern (Fig. 5). Both structures (Figures 1 and 6) have been refined on the basis of single crystal X-ray data.

Interestingly the high-temperature phase has a smaller volume (65.3 Å^3 per formula unit) than the low-temperature form (67.3 Å^3). This behavior has also been observed for the dimorphic compounds GdNiSb (LT-MgAgAs and HT-AlB_2 type structure) [20] and YbAuBi (LT-MgAgAs and HT-LiGaGe type structure) [6]. All the HT-phases crystallize with structures of the well known AlB_2 family [26]. It is important to note that the phase transitions for all three compounds are reconstructive, leading to significantly different coordinations in the high-temperature modifications. Here we discuss the differences in the structures of LT- and HT-YbPdSb. Both modifications are built up from three-dimensional [PdSb] networks with regular $PdSb_{4/4}$ tetrahedra in LT-YbPdSb and strongly distorted tetrahedral in HT-YbPdSb (see Figures 1 and 6). The most significant difference occurs for the average Pd-Sb distances of 280 and 272 pm in LT- and HT-YbPdSb, respectively. In HT-YbPdSb the Pd-Sb distances are only slightly larger than the sum of the covalent radii of 269 pm [37]. We can thus assume stronger Pd-Sb bonding in the high-temperature modification.

The second difference concerns the coordination of the ytterbium atoms. In LT-YbPdSb each ytterbium atom has four palladium neighbors in tetrahedral and six antimony atoms in octahedral coordination. The shortest Yb-Yb contacts are at

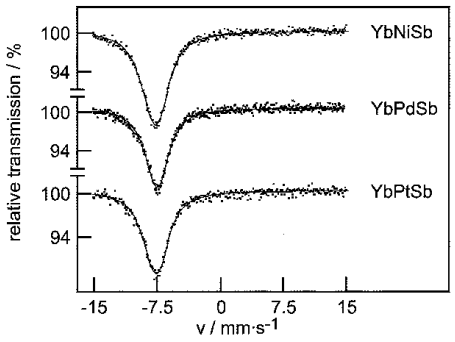

Fig. 8. Experimental and simulated ^{121}Sb Mössbauer spectra of Yb*T*Sb (*T* = Ni, Pd, Pt) at 78 K.

457 pm and should not be considered as bonding. The twelve nearest ytterbium neighbors form a cuboctahedron around each ytterbium atoms (*fcc* arrangement). The high temperature modification has a higher coordination number of the ytterbium atom: 6 Pd (ø 325 pm) + 6 Sb (323 pm) + 4 Yb (369 and 397 pm). Here, the Yb-Yb distances are significantly shorter than in the LT-modification. They compare well with the Yb-Yb distance of 389 pm in *fcc* ytterbium [38]. From the comparison of the interatomic distances we can conclude stronger Pd-Sb bonding in HT-YbPdSb but stronger Yb-Pd bonding in LT-YbPdSb. For a more detailed discussion of the crystal chemistry and chemical bonding of MgAgAs and TiNiSi type intermetallics we refer to two recent reviews [24, 26, and ref. therein].

The change in crystal structure is accompanied by a change of the ytterbium valence. According to the magnetic susceptibility data [3, 18], LT-YbPdSb is Curie-Weiss paramagnetic, although the cell volume slightly deviates from the lanthanoid contraction [39]. This is consistent with essentially trivalent ytterbium. In the high-temperature phase the ytterbium atoms have the higher coordination number indicating a larger space requirement. Since our quenching experiments always resulted in mixtures of LT-YbPdSb and HT-YbPdSb it was not reasonable to carry out magnetic susceptibility measurements. Nevertheless, from the structural change we assume that ytterbium is essentially divalent in the HT modification. This is also the case in HT-YbPdSn [40] which is isotypic with the antimonide. In contrast, in cubic YbAuBi the Yb atoms are divalent [41]. The magnetic properties of the high-temperature phase are not known. These findings manifest that the magnetic ground state of ytterbium in the Yb*TX* compounds strongly depends on the strength of the *f-d* and *f-p* hybridizations.

Table 7. Fitting parameters of ^{121}Sb Mössbauer measurements on the antimonides Yb*T*Sb (*T* = Ni, Cu, Pd, Ag, Pt, Au). δ: isomer shift, Γ: linewidth, ΔE_Q: electric quadrupole interaction.

Compound	δ / mm·s^{-1}	Γ / mm·s^{-1}	ΔE_Q / mm·s^{-1}
YbNiSb	–7.42(5)	2.8(2)	0.5(1)
YbCuSb	–7.44(4)	2.8(1)	0.4(1)
YbPdSb	–7.34(5)	2.9(3)	0.4(2)
YbAgSb	–7.76(7)	3.0(2)	0.5(1)
YbPtSb	–7.36(7)	2.7(3)	0.5(2)
YbAuSb	–7.82(5)	2.7(2)	0.2(1)

^{121}Sb Mössbauer spectroscopy

The ^{121}Sb Mössbauer spectra of Yb*T*Sb (*T* = Ni, Pd, Pt, Cu, Ag, Au) are presented in Figures 7 and 8. The fitting parameters are listed in Table 7. All spectra show single signals as expected from the single crystallographic antimony sites. The isomer shifts range from –7.34(5) to –7.82(5) mm/s with experimental line widths between 2.7(2) and 3.0(2) mm/s. Although the nickel based samples showed at least 10% of a distribution of $YbNi_xSb$ besides YbNiSb, there is no indication for this behavior from the ^{121}Sb spectra. The natural line width is too large to observe small differences in the spectra.

Acknowledgements

We thank Dr. H. Piotrowski (LMU München) for an intensity data collection and the Degussa-Hüls AG for a generous gift of noble metals. This work was financially supported by the Fonds der Chemischen Industrie and by the Deutsche Forschungsgemeinschaft. R. M. is indebted to the Alexander von Humboldt Foundation for a postdoctoral stipend.

[1] A. E. Dwight, Proc. Rare Earth Res. Conf. **2,** 642 (1974).
[2] R. Marazza, D. Rossi, R. Ferro, J. Less-Common Met. **75,** P25 (1980).
[3] S. K. Dhar, N. Nambudripad, R. Vijayaraghavan, J. Phys. F: Met. Phys. **18,** L41 (1988).
[4] F. G. Aliev, V. V. Moshchalkov, V. V. Kozyrkov, M. K. Zalyalyutdinov, V. V. Pryadun, R. V. Scolozdra, J. Magn. Magn. Mater. **76&77,** 295 (1988).
[5] F. G. Aliev, G. I. Pak, T. M. Shkatova, Sov. Phys. Solid State **31,** 1615 (1989).
[6] F. Merlo, M. Pani, M. L. Fornasini, J. Less-Common Met. **166,** 319 (1990).
[7] M. Kasaya, H. Suzuki, T. Yamaguchi, K. Katoh, J. Phys. Soc. Jpn. **61,** 4187 (1992).
[8] H. Suzuki, T. Yamaguchi, K. Katoh, M. Kasaya, Physica B **186-188,** 390 (1993).
[9] S. K. Dhar, K. A. Gschneidner Jr., R. Vijayaraghavan, Physica B **186-188,** 463 (1993).
[10] G. Le Bras, P. Bonville, P. Imbert, G. Polatsek, M. J. Besnus, P. Haen, V. Moshchal'kov, Physica B **199&200,** 542 (1994).
[11] F. G. Aliev, S. Vieira, R. Viiar, M. Kasaia, H. Sutsuki, R. Vonvibe, Pis'ma Zh. Eksp. Teor. Fiz. **60,** 714 (1994).
[12] M. Kasaya, K. Katoh, H. Suzuki, Tohoku Daigaku Kinzoku Zairyo Kenkyusho Kyojiba Chodendo Zairyo Kenkyu Senta Nenji Hokoku, 228 (1994).
[13] A. K. Solanki, A. Kashyap, S. Auluck, M. S. S. Brooks, J. Appl. Phys. **75,** 6301 (1994).
[14] G. Le Bras, P. Bonville, M. J. Besnus, P. Haen, P. Imbert, G. Polatsek, F. G. Aliev, Physica B **206&207,** 338 (1995).
[15] G. Le Bras, P. Bonville, J. A. Hodges, J. Hammann, M. J. Besnus, G. Schmerber, S. K. Dhar, F. G. Aliev, G. Andre, J. Phys.: Condens. Matter **7,** 5665 (1995).
[16] H. Suzuki, M. Kasaya, M. Kohgi, A. Dönni, P. Fischer, G. Le Bras, P. Bonville, Physica B **206&207,** 341 (1995).
[17] K. Katoh, T. Takabatake, A. Minami, I. Oguro, H. Sawa, J. Alloys Compd. **261,** 32 (1997).
[18] P. Bonville, G. Le Bras, P. Dalmas de Réotier, A. Yaouanc, R. Calemczuk, C. Paulsen, M. Kasaya, F. G. Aliev, Physica B **230&232,** 266 (1997).
[19] H. Flandorfer, K. Hiebl, C. Godart, P. Rogl, A. Saccone, R. Ferro, J. Alloys Compd. **256,** 170 (1997).
[20] R. V. Skolozdra, A. Guzik, A. M. Goryn, J. Pierre, Acta Phys. Pol. **92A,** 343 (1997).
[21] P. Larson, S. D. Mahanti, S. Sportouch, M. G. Kanatzidis, Phys. Rev. B **59,** 15660 (1999).
[22] S. Sportouch, P. Larson, M. Bastea, P. Brazis, J. Ireland, C. R. Kannewurf, S. D. Mahanti, C. Uher, M. G. Kanatzidis, Mater. Res. Soc. Symp. Proc. **545,** 421 (1999).
[23] T. Takabatake, Y. Bantou, Jpn. Kokai Tokkyo Koho Pat. No. JP 2000332308, A2, 20001130 (2000).
[24] R. Pöttgen, D. Johrendt, D. Kußmann, in K. A. Gschneidner (Jr.), L. Eyring (eds.): Handbook on the Physics and Chemistry of Rare Earths, chapter 207, vol. 32, 453-513 (2001).
[25] G. Wenski, A. Mewis, Z. Kristallogr. **176,** 125 (1986).
[26] R.-D. Hoffmann, R. Pöttgen, Z. Kristallogr. **216,** 127 (2001).
[27] C. B. Shoemaker, D. P. Shoemaker, Acta Crystallogr. **18,** 900 (1965).
[28] H. Nowotny, W. Sibert, Z. Metallkd. **33,** 391 (1941).
[29] R. E. Bodnar, H. Steinfink, Inorg. Chem. **6,** 327 (1967).
[30] R. Pöttgen, Th. Gulden, A. Simon, GIT-Laborfachzeitschrift **43,** 133 (1999).
[31] R. Pöttgen, A. Lang, R.-D. Hoffmann, B. Künnen, G. Kotzyba, R. Müllmann, B. D. Mosel, C. Rosenhahn, Z. Kristallogr. **214,** 143 (1999).
[32] K. Yvon, W. Jeitschko, E. Parthé, J. Appl. Crystallogr. **10,** 73 (1977).
[33] G. M. Sheldrick, SHELXS-97, Program for the Solution of Crystal Structures, University of Göttingen, Germany, 1997.
[34] G. M. Sheldrick, SHELXL-97, Program for Crystal Structure Refinement, University of Göttingen, Germany, 1997.
[35] F. Hund, R. Fricke, Z. Anorg. Allg. Chem. **258,** 198 (1949).
[36] E. Zintl, G. Brauer, Z. Elektrochem. Angew. Phys. Chem. **41,** 297 (1935).
[37] J. Emsley, The Elements, 3rd edn, Oxford University Press, Oxford (1999).
[38] J. Donohue, The Structures of the Elements, Wiley, New York (1974).
[39] S. K. Malik, D. T. Adroja, J. Magn. Magn. Mater. **102,** 42 (1991).
[40] D. Kußmann, R. Pöttgen, B. Künnen, G. Kotzyba, R. Müllmann, B. D. Mosel, Z. Kristallogr. **213,** 356 (1998).
[41] D. Kaczorowski, A. Leithe-Jasper, P. Rogl, H. Flandorfer, T. Cichorek, R. Pietri, B. Andraka, Phys. Rev. B **60,** 422 (1999).